Data-Driven Approach to Modeling and Development of a 30 kW Field-reversed Configuration Thruster

IEPC-2019-717

Presented at the 36th International Electric Propulsion Conference
University of Vienna, Austria
September 15–20, 2019

Joshua M. Woods,[*] Christopher L. Sercel,[†] Tate M. Gill,[‡] Eric Viges,[§] and Benjamin A. Jorns[¶]
University of Michigan, Ann Arbor, Michigan, 48109, United States of America

A 30 kW Field-reversed configuration thruster is currently in development in the Plasmadynamics and Electric Propulsion lab. The thruster will be operated at steady state to produce reliable thrust measurements that can be used to validate a theoretical mutual inductance model for coupling between the coils and plasmoid as well as to calibrate an empirical performance model capable of predicting thrust and serving as a basis for optimization.

Nomenclature

g = gravitational constant

[*]Ph.D Candidate, Aerospace Engineering, jmwoods@umich.edu.
[†]Ph.D Candidate, Aerospace Engineering, csercel@umich.edu
[‡]Master of Science in Engineering Student, Aerospace Engineering, tategill@umich.edu
[§]Research Engineer, Aerospace Engineering, eviges@umich.edu
[¶]Assistant Professor, Aerospace Engineering, bjorns@umich.edu

I. Introduction

The domain of high power propulsion traditionally has been dominated by chemical rockets which provide high thrust, but whose low specific impulse (I_{sp}) translates to poor use of propellant mass. Because I_{sp} directly limits the maximum Δv that a propulsion system can achieve with a given mass fraction, missions destined for high Δv targets are required to carry a propellant load many times more massive than the payload. Plasma propulsion techniques allow for exhaust velocities orders of magnitude higher than chemical devices and therefore commensurately higher I_{sp} [1]. Currently, Hall thrusters are becoming the workhorse plasma propulsion device. They can achieve I_{sp}s of 10^3 s with efficiency over 60% [2]. However, most Hall thrusters are only capable of power levels in the single kilowatts. Current efforts are underway to scale Hall thrusters up to as much as 100 kW [3], but given current trends in solar panel technology [4], it is likely that the domain of MW-level electric propulsion technology will soon be open to us. To further increase mission scope given an initial launch mass, it is also desirable that the next generation of thrusters demonstrate in-situ resource utilization (ISRU) by the capability to refuel mid-mission using propellants found in space [5]. This presents a significant challenge because the most common ISRU propellants, carbon dioxide and water, become highly oxidative when they dissociate at high temperatures. This necessitates that any ISRU-compatible thruster be strongly resistant to lifetime-limiting erosion. The need is apparent for a next generation thruster scalable up to MW power and compatible with ISRU propellants.

A promising candidate to fill this role is the Field-Reversed Configuration (FRC) thruster. An FRC is a type of compact toroidal plasmoid studied by the fusion community since the late 1950s for its remarkably long confinement time given its simple magnetic geometry relative to other fusion devies [6]. These plasmoids are characterized by an axial magnetic field whose sign is reversed near the axis by azimuthal currents induced in the plasma by one of several techniques, such as a rotating radial magnetic field (RMF) [7]. The plasma forms a toroid with closed magnetic field lines. Thrust can be produced by introducing a radial component to the magnetic field which interacts with the azimuthal current in the plasma via the Lorentz force. The thruster is operated in a pulsed mode, repetitively forming and accelerating FRC plasmoids [8].

The FRC's unique method for generating thrust provides a number of advantages compared to state of the art high-power concepts. The confinement of the plasmoid reduces contact with thruster walls and the inductive coupling eliminates the issue of electrode wetting, making the device agnostic to propellant species. Theoretically, there are limits on current density in the plasmoid, which allows for up to MW-level power in a device 10s of cm in cross-section [9] with potential power scaling up to 20 kW/kg [10], compared to Hall thrusters at approximately .5 kW/kg [11]. The closed nature of the magnetic field lines in the FRC plasmoid mean that no B-field detachment is necessary in the plume, avoiding a common efficiency loss in plasma propulsion systems.

Although these devices have been built and operated successfully in the past by the Air Force Research Lab and Michigan Technical University [12], NASA Marshall [13], and the private company MSNW LLC [8,14], published performance measurements are lacking, and many basic questions regarding the acceleration of the plasmoid have not been answered. No direct published thrust measurements have yet been performed on an RMF-FRC, for example. Measurements that have been taken indirectly indicate poor performance for these devices [8]. In light of these open challenges, there is a pressing need for a dedicated experimental study of the performance of such a thruster.

In parallel with this need, there is an equally important interest in being able to develop an improved understanding and model for these devices. This is critical for guiding efforts to improve performance. To thi end, in previous work, we derived a lumped-circuit model for an RMF thruster to to address basic questions of the acceleration mechanism. This yielded interesting insight into operation such as X an Y and z. However, as a reduced fidelity model, we recognized in this previous work that there are inherent limitations to its accuracy. Most notably, it is necessary to lump complex and potentially non-linear processes into scalar terms. A noteable example, as is consistent with many previous treatments of pulsed plasma systems (cite Polzin, Hill, Eskridge, etc.) here is to represent the interaction of the plasma with the external coils via an unspecified mutual induction. This is a critical parameter governing efficiency and thrust. While we have have attempted to motive simple analytical expressions for this mutual inductance in our previous work, we recognize that absent higher fidelity simulations, this parameter only can truly be inferred from measurement. This is in keeping with the work of Kirtley et al. A knowledge, even empirically informed, of how this mutual inductance varies for operating condition is critical for not only being able to re-create the performance of a system but also potentially to guide optimization studies. With this in mind, the demand for validation data in turn points to the need for a highly configurable experimen. Ideally, performance measurements taken over a wide range of operating parameters (magnetic field strengths, input energy, pulse rate, and mass flow rates) would allow us to also calibrate an empirical performance model for steady state thrust.

In light of the need for the first direct performance measurements of an RMF-FRC system coupled with the complementery interest in improving our understanding of the operation of these devices through semi-empirical models, we present in this paper the design for an RMF-FRC thruster currently under construction at the Uiversity of Michigan. To this end, we begin with a description of RMF-FRC theory. In the following study, we review RMF-FRC theory. We discuss our current performance model in the context of thruster operation and introduce a framework for determining key thruster scaling empirically and thus forming the basis for optimizing future thrusters. We then discuss requirements for our test article and detail each subsystem of the thruster and conclude with a brief overview of our upcoming experimental campaign.

II. RMF-FRC Thrust Mechanism

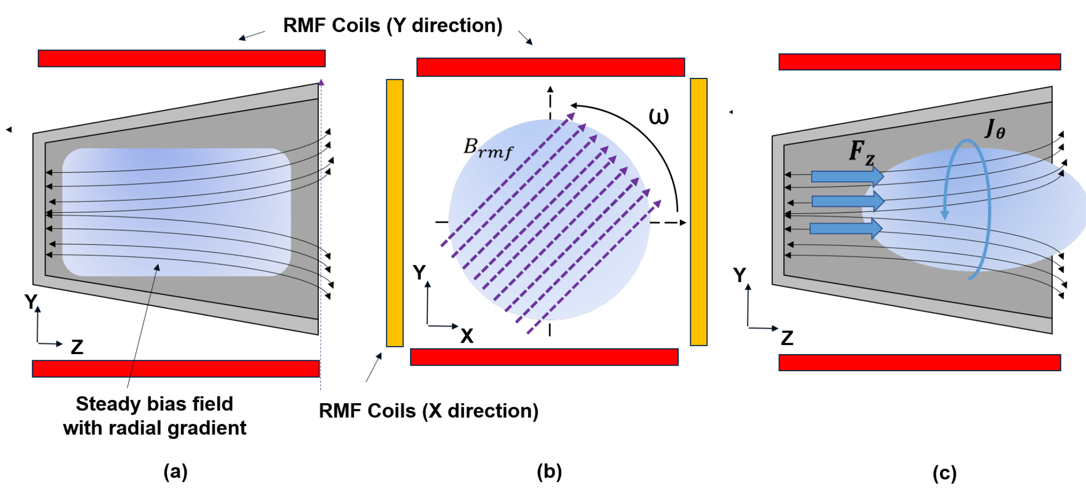

Fig. 1 RMF-FRC Operation - (a) Ionized gas is injected into the thruster cone. A steady bias magnetic field with a radial gradient is present. (b) Two sets of coils oriented in the x and y directions are used to generate a rotating magnetic field (RMF) by driving sinusoidal currents 90°out of phase at frequency ω. The RMF induces axial and azimuthal currents. (c) The FRC is formed. Large azimuthal currents in the plasma interact with the external radial magnetic field which drives the plasmoid out of the thruster via the Lorentz Force.

We consider here an idealized case for RMF-FRC operation to illustrate the fundamentals of their operation as illustrated in Figure 1. RMF-FRCs operate by inducing azimuthal currents in a plasma column confined by a steady background axial magnetic field. At a threshold value, the magnetic field resulting from the flowing azimuthal current reverses the background axial field near the plasma centerline, resulting in a self-contained magnetic structure populated by a high density plasma. This magnetic plasmoid is then accelerated by a Lorentz force that results when the azimuthal currents in the plasmoid interact with a gradual radial gradient in the background field. Fig. 1 illustrates the process. Ionized gas fills the thruster chamber with a background steady magnetic field of the form

$$\vec{B}_s = B_{s,r}\hat{r} + B_{s,z}\hat{z}, \tag{1}$$

where $B_{s,r}$ and $B_{s,z}$ are the radial and axial components of the bias field respectively. Two sets of coils arranged perpendicular to each other alternating magnetic fields 90°out of phase. The combined effects of each coil creates a rotating magnetic field of the form

$$\vec{B}_{RMF} = B_o\cos(\omega t - \theta)\hat{r} + B_o\sin(\omega t - \theta)\hat{\theta} = B_{r,ext}\hat{r} + B_{\theta,ext}\hat{\theta}, \tag{2}$$

where B_o is the amplitude of the magnetic field and ω is the frequency at which the field rotates. This is an idealized RMF. The fields have no radial or axial dependence. In our model, we assume the RMF is the idealized form presented by equation 2. This is to illustrate qualitatively the performance of the devices in order to find a simplified form for the B-field. We note that this form of the field is relaxed in a more self-consistent analysis. We assume that they are not affected by the loading of the plasma during discharge and maintain a sinusoidal θ dependence. The only effects of plasma loading on the RMF is due to the change in magnitude of their currents. Using Faraday's law of induction and the generalized Ohm's law for an infinitely long plasma column with negligible axial and azimuthal pressure gradients, the time varying magnetic field produces an electric field that drives an axial and azimuthal current,

$$J_z(t,r,\theta) = \frac{\omega r B_{r,ext}}{\eta} - \frac{ne\omega r(B_{r,ext} + B_{s,r}\hat{r})}{\eta ne\left(1 + 2\left(\frac{\eta ne}{B_o}\right)^2\right)}, \tag{3}$$

$$J_\theta(t,r) = -\frac{ne\omega r}{1 + 2\left(\frac{\eta ne}{B_o}\right)^2}, \tag{4}$$

where n is the electron density (assumed to be constant in this study) e is the elementary charge, and η is the resistivity defined as

$$\eta = \frac{m\nu_{ei}}{ne^2}. \tag{5}$$

Here, ν_{ei} is the electron-ion collision frequency and m is the mass of an electron. At a sufficiently high magnetic field magnitude, the electrons become fully tied and rotate synchronously with the field lines, thus reducing equation 4 to:

$$J_\theta(t,r) = -ne\omega r \tag{6}$$

The azimuthal current interacts with the radial component of the steady bias field to produce an axial Lorentz force that drives the plasmoid out of the thruster at high speeds:

$$F_z = \int_V J_\theta B_{s,r} dV \tag{7}$$

The repeated formation and ejection of the plasmoid under the axial force (equation 7) at sufficiently high pulse rates creates quasi-steady state thrust.

III. Performance Model

A. Review of FRC Circuit Models

Here we expand upon our lumped circuit performance model previous detailed in[15]. Included in the model is an expression of the coupling between the RMF coils and the plasmoid. It provides insight into the energy transfering mechanism between the coils and is critical in our understanding of thruster operation. In Section IV, we discuss how we wish to calibrate the mutual inductance expression based on operational data. Additionally, we nondimensionalize the circuit equations to identify key scaling parameters which we can use to help guide our design process.

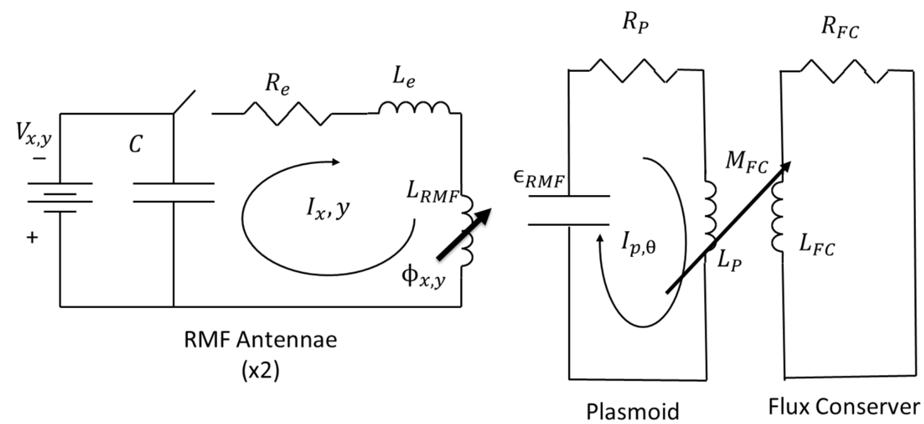

Fig. 2 Lumped circuit of an RMF-FRC

There is a long history of modeling pulsed EP devices as lumped circuits to identify key performance scaling, mainly specific impulse and efficiency as a function of initial input energy. Typical models simplify the driving circuit as a charged capacitor in series with resistance and an inductor representing the induction coil coupled to a conducting slug representing the plasma body with its own self inductance and plasma. A critical parameter describing the behavior of the thrusters using this technique is the mutual inductance between the accelerating coils and the plasmoid. Mutual inductance has been studied and modeled extensively for electromagnetic inductors[16]. J. Bernades and S. Merryman provided an empirical expression for mutual inductance as a function of position for ring shaped conductors accelerated by a driving coil. The expression was derived by directly measuring the mutual inductance at various positions and fitting a curve to the data points[17]. While calculated for ring shaped inductors, the mutual inductance model coupled with a lumped circuit was shown to reasonably predict performance of pulsed plasmoid thrusters utilizing various geometries[18]. Furthermore, Hill used the mutual inductance expression to predict performance of annular FRC's (AFRC)[19,20]. Nevertheless, there are several shortcomings and questions regarding antennae-plasmoid coupling for RMF-FRC's that we wish to investigate. As opposed to the model presented by J. Bernades and S. Merryman, we wish to directly model the mutual inductance by calculating flux expressions caused by the plasmoid onto the RMF antennae resulting in back emf and ultimately affecting the coil and plasma currents. Such methods were successfully used to model the plasma currents and RMF penetration into the plasmoid by W. N. Hugrass et al[21]. However, the circuit model used by the authors was for fusion purposes and did not include the effects of the plasmoid translating through the inductive region. We attempt to model such effects in this study. J. Little et al used a lumped circuit to model a potential second stage for an RMF-FRC consisting of a series of flux coils downstream of the RMF coils. The flux coils are pulsed as the plasmoid traverses downstream, adding energy to the plasma body[22]. Expressions for the mutual inductance were derived using plasma current equilibrium expressions derived by Solov'ev[23]. Thus, expressions for the flux produced by the plasmoid during its acceleration in the RMF region are still unknown.

B. Performance Model Equations

In 2018, we derived a performance model by simplfying the thruster as a lumped circuit and modeling the plasmoid as a simple conducting slug of fixed cylindrical geometry and constant, uniform density[15]. Here, we expand upon that model by adding the effects of the flux conservers which are used to recapture energy as the plasmoid accelerates through the thruster. The full circuit is shown in figure 2. Key assumptions we employ in this analysis include

- Uniform density in r-θ
- Semi-infinite plasma in axial direction
- Constant background magnetic field with radial gradient
- Cold plasma
- Etc.

We first introduce a series non-dimensionalized governing equations are given by :

$$I_j{}^* = \tfrac{1}{V_o}\sqrt{\tfrac{L_{RMF}}{C}}I_j \qquad I_{P,\theta}{}^* = \tfrac{1}{V_o}\sqrt{\tfrac{L_{RMF}}{C}}I_{P,\theta} \qquad I_{FC}{}^* = \tfrac{1}{V_o}\sqrt{\tfrac{L_{RMF}}{C}}I_{FC}$$

$$V_j{}^* = \tfrac{1}{V_o}V_j \qquad \epsilon_{RMF}{}^* = \tfrac{1}{V_o}\epsilon_{RMF} \qquad \phi_j{}^* = \tfrac{1}{(L_e+L_{RMF})V_o}\sqrt{\tfrac{L_{RMF}}{C}}\phi_j$$

$$t^* = \tfrac{1}{\sqrt{(L_e+L_{RMF})C}}t \qquad z^* = \tfrac{1}{z_o}z \qquad M_{FC,P}{}^* = \tfrac{1}{L_{FC}M_{FC,P}}$$

Physically, these reprsent X and Y. Armed with these results, we can show through application of Biot-Savart and Kirchoff's laws (Appendix) the following key governing equations for the equivalent circuit.

1. Voltage in RMF coil

$$V_j{}^*(t^*) + \frac{1}{Q_{RMF}}I_j{}^*(t^*) + \sqrt{1+L^*}\frac{dI_j{}^*(t^*)}{dt^*} = \frac{k}{\sqrt{1+L^*}}\frac{d\Phi_j{}^*(t^*)}{dt^*} \tag{8}$$

$$\frac{dV_j{}^*(t^*)}{dt^*} = \sqrt{1+L^*}I_j^*(t^*) \tag{9}$$

$$\phi_j{}^*(t^*) = \frac{M_{RMF,P}(t^*)}{L_{RMF}}\left[-\frac{dI_j{}^*(t^*)}{dt^*} + \frac{\Omega(t^*)^2}{2\big(1+\Omega(t^*)^2\big)}I_j{}^*(t^*)\right] \tag{10}$$

Talk about what it means here. We physically also have introduced a mutual inductance term that accounts for X and Y. historically, this mutual inductance has not been determined from first principles. For other pulsed inductive systems it is is measured empirically.

2. Voltage in induced azimuthal current in plasma

$$Q_P I_{P,\theta}{}^*(t^*) + \frac{L_P}{L_{RMF}}\frac{1}{\sqrt{1+L^*}}\frac{d\big(I_{P,\theta}{}^*(t^*)\big)}{dt^*} + \frac{1}{\sqrt{1+L^*}}\frac{d\big(M_{FC,P}{}^*(t^*)I_{FC}{}^*(t^*)\big)}{dt^*} = \epsilon_{RMF}(t^*) \tag{11}$$

3. Voltage induced in flux conservers by plasma currents

$$Q_{FC}I_{FC}^*(t^*) + \frac{dI_{FC}^*(t^*)}{dt^*} = \frac{d\big(M_{FC,P}^*(t^*)I_P^*(t^*)\big)}{dt^*} \tag{12}$$

4. Acceleration of FRC

$$\frac{d^2 z^*(t^*)}{dt^{*2}} = \alpha_{RMF}\frac{(1-z^*(t^*))}{\Big[1+\Omega(t^*)^2\Big]}\Big(\frac{dI_x^*(t^*)}{dt^*}I_y^*(t^*) - I_x^*(t^*)\frac{dI_x^*(t^*)}{dt^*}\Big) + \alpha_{FC}I_{P,\theta}^*(t^*)I_{FC}^*(t^*)\frac{dM_{FC,P}^*(t^*)}{dz^*(t^*)} \tag{13}$$

Has two effects: linear with j and quadratic with j. Why does it have these and what do they mean? The former is due to the Lorentz interaction with the background magnetic field of the current induced by the RMF effect, the latter (on the RHS of acceleration term) is the consequence of the interaction of the magnetic field from the circulating current plasma interacting with the induced current in the flux conservers. This is an interesting departure from classical pulsed inductive devices in which azimuthal currents in the circuit induce current in the plasma.

The above results represent a solvable simplified circuit model for the RMF-FRC thruster. The structure mirrors that of other pulsed plasma work (cite all), though with significant depatures that account for the unique configuration of an RMF-FRC circuit. hese include the need to account for multiple pulsing circuits and the interesting physical result that there are both linear and nonliner contributions in current with thrust that stem from the flux conservers. The fact that there are two pulsers and flux conservers increases the number of governign equations. Indeed, in contrast to the canonical pulsed inductive formulations (Polzin) where two-three equations are sufficient, we have X.

With that said, as is consistent with previous work, in order to arrive at this simplified formulation, it has been necessary to lump the magnetic effects (which ultimately are critical for driving the acceleration) into scalar mutual inductance terms (label and equation). These flux terms defined in equations 12 and 13 are the crux of our model. They define how the RMF antennae couples energy into the plasma. Unfortunately, an as aluded to in the preceding, we do not have rigorous first principles models for these coupling terms. This is the major trade in adopting the simplified circuit model: the sacrifice in fidelity eliminates a predictive capability. Thus, this model cannot in its current form be used to drive insight in to thruster operation. As discussed in the introduction, this type of insight is critical for complementing our efforts to understand exiting performance limitations and optimize the thruster.

With this in mind, we discuss in the next section our approach to filling in the knowledge gap related to the mutual inductance.

IV. Data-driven approach to determining the mutual inductances in lump circuit model

A. Approach

The problem of determining mutual inductance is a common problem for equivalent circuit modeling of pulsed inductive devices. In an effort to overcome thisk previous studies have explored developing simplified models for the mutual indutance informed by simplified electromagnetic modeling or experiment. A similar approach has been applied to FRCs (Kirtley). Recognizing the copmlexity of an RMF-FRC system, we ultimately elect to follow an experimental approach as well. The goal is to try to use data to find expressions for these results that functionally depend on key parameters of the thruster geometry and operating condition. If these simplified results can be determined empirically and validated, they can close the governing equations (see previous section), allowing for a self-consistent calculation.

With this in mind, we intend to use a data-driven approach for determing these mutual inductances (M(position, geometry,e tc) (much as was done by Polzin and Hill). To this end, we require a test article that we can parametrically vary, monitoring its performance and circuit ring down. The idea is to tune the mutual inductances in Eqs. x-y to match these results. If we can parmaetrically vary the operating conditions over a wide enough envelope, we should be able to generate datasets of the mutual inductance as a function of operating condition (power, pulse rate) and thruster geometry. This in turn will help us to regress this dataset, identifying functional forms for the mutual inductances.

B. Base functions for regression

The parameter space of FRC operation is large and this naturally begs the question as to what the appropriate basis expressions should be explored for the functional forms of the mutual inductance. To guide this approach, we can leverage a number of known well non-dimensional parameters for pulsed inductive systems, making the ansantz that these will be the critical parameters:

These include

$$E_o = C{V_o}^2 \tag{14}$$

$$\omega_o = \frac{1}{\sqrt{(L_e + L_{RMF})C}} \tag{15}$$

Using these definitions, we can define our scaling parameters beginning with the Q-factors for the RMF antennae, plasmoid, and flux conserver respectively:

$$Q_{RMF} = \frac{1}{R_{RMF}}\sqrt{\frac{C}{L_e + L_{RMF}}} \tag{16}$$

$$Q_P = \frac{1}{R_{P,eff}}\sqrt{\frac{C}{L_RMF}} \tag{17}$$

$$Q_{FC} = \frac{1}{R_{P,eff}}\frac{\sqrt{(L_e + L_{RMF})C}}{L_RMF} \tag{18}$$

These values represent the damping response for each of the conductors in the system. We next define:

$$L^* = \frac{L_e}{L_{RMF}} \tag{19}$$

which is the ratio of energy lost to the parasitic resistance in the RMF lines to the energy used in the RMF antennae. It should be minimized while the Q factor should be maximized to reduce energy losses in the power lines. Lastly we define two force scaling parameters for equation 33 for the RMF and flux conserver contributions respectively:

$$\alpha_{RMF} = \frac{1}{m_{bit} z_o {\omega_o}^2}\frac{\pi r p^3 \gamma^2}{2\eta^2 ne}\frac{E_o}{L_{RMF}\omega_o} \tag{20}$$

$$\alpha_{FC} = \frac{E_o {\omega_o}^2}{m_{bit} {z_o}^2}\frac{L_{FC}}{L_{RMF}} \tag{21}$$

The central idea here is that we anticipate the mutual inductance should depend on these parameters. And indeed, when we regress the data, we anticipate that it will have a form of the type:

C. Proof of concept

As a proof of concept for this approach, we actually drived in 2018 a simplified model for the mutual inductance in the RMF-FRC The key assumptions were X, Y, and Z leading to the following expression

$$M_{RMF,P}(t) = \frac{r_p(3{r_c}^2 + r_p)\gamma\mu_o(z_o - z(t))}{3\sqrt{2}\eta} \tag{22}$$

We also follow Eskridge and others in identifing a semi-empirical expression for the coupling with the flux conservers:

$$M_{FC,P}(t)\sqrt{L_{FC}L_P}exp\Big(-\frac{z(t)}{z_o}\Big). \tag{23}$$

If we assume some fixed value of z_0, we can use these result in conjunction with the governing equations to solve for the circuit ring down and performance of the system. We show a sample result for ring down and performance for input parameters X, Y, and Z in Fig. X. Physically, if this mutual inductance term were correct, we these are the performance metrics and circuit properties we would measure.

As a demonstration of a data-driven approach, we can use this simplified model to approximate how a "real" thruster's operation would parametrically vary. To this end, we use these expressions and run model multiple times for different input parameters. For each run, we "measure" the mutual inductances from the output by assuming that each

Although this is a simply demonstration, it illustrates the general approach we propose to apply here. Armed with this validation, the intention is to be able to leverage these same techniques to apply this approach to a real thruster. We discuss in the next section the design of a thruster to satisfy this end.

V. Thruster Design

A. Thruster Requirements

Need to also mention in here how it will have flexibility to help tune model The scaling parameters derived in section IV. help guide our thruster design. First, as with other pulsed inductive devices, it is imperative that we minimize any stray inductance, per L^*, and maximize the Q-factor of the RMF antennae, per Q_{RMF}. To this end, we require that the stray inductance be at most an order of magnitdue less than the inductance of the RMF antennae. Next, the resonant frequency of the system, which dictates the magnitude of azimuthal current per equation 4, must be between the ion and electron cyclotron frequencies to entrain the electrons but not the ions. As such, for a plasmoid density of $10^{19}m^{-3}$ and a resistivity of 10^{-5}, we target a frequency of approximately 20 kHz. In addition, the magnitude of the RMF must be sufficient to entrain the electrons throughout the acceleration process. From the literature and our own Spice modeling of the thruster, we target a peak magnetic field of 350 G. For quasi-steady state thrust that can be effectively measured on a thrust stand, we target a pulse rate of 1 kHz. Finally, any supporting infrastructure for the thruster must be compatible with the Large Vacuum Test Facility at the Plasmadynamics and Electric Propulsion Lab and the power processing unit will be placed outside of the chamber.To achieve these requirements, thruster subsystem designs are detailed below.

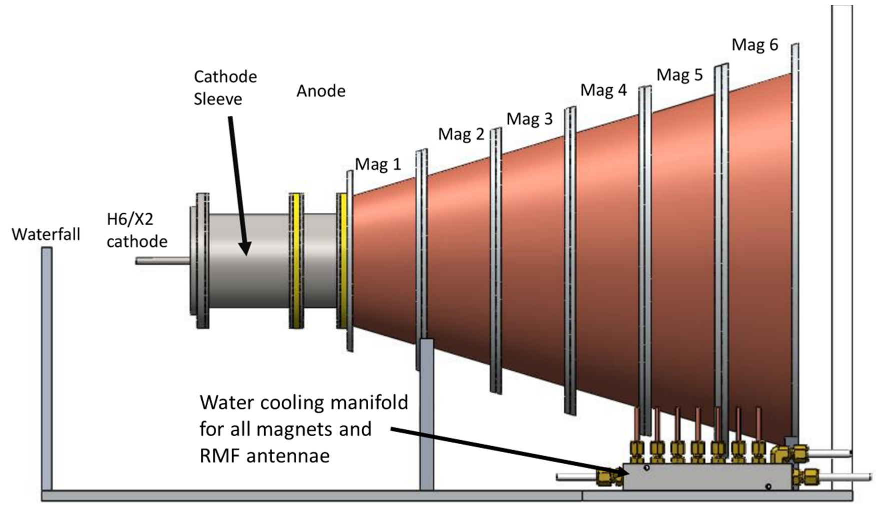

h

Fig. 3 CAD of the thruster on its mounting plate

B. Plasma Source

Because one of the major needs the FRC thruster seeks to satisfy is ISRU-compatibility, groups which have built these devices in the past have sought to design the entire thruster as electrodeless. This lends itself toward inductive pre-ionization schemes which must be pulsed. Additionally, facility constraints have required puffed gas release through the pre-ionization mechanism. This combines to result in a puffed, pulsed pre-ionization scheme with multiple steps that must be triggered correctly with each other and with the RMF antennas. Significant time has been put into developing pre-ionization schemes for past FRC thrusters [10]. However, our goals are to study the FRC formation and acceleration mechanisms and to make measurements of thrust and specific impulse, none of which depend on the pre-ionization source being ISRU-compatible. Additionally, the Large Vacuum Test Facility (LVTF) at the University of Michigan has a Xe pumping speed of 500,000 l/s, allowing for constant propellant flow without risk of overcoming the vacuum pumps. Therefore, we can dramatically reduce the engineering complexity of the system as a whole by using a tried-and-true plasma source to fill the RMF cone with a pre-ionized gas – the LaB6 hollow cathode. A Lanthinum Hexaboride (LaB6) hollow cathode functions by heating a cylindrical piece of LaB6 to cause thermionic emission, then striking a discharge between the insert and a nearby keeper electrode once the insert is emitting enough electrons. After the initial discharge is struck, voltage can be applied between the cathode and the anode, which is large enough to accept the full discharge current without overheating. Magnetic fields prevent electrons from streaming directly to the anode, increasing ionization efficiency.

In our case, we use the hollow cathode originally developed for the X2 Hall thruster, operating with approximately 100 sccm Xe flow combined between the cathode and the neutral diffuser. The neutral diffuser provides an azimuthally-symmetric flow of neutral gas. The magnetic fields to prevent immediate electron streaming to the anode are provided already by the bias coils. This should provide similar pre-ionization conditions as Weber's 'standard shot' [10], which we use as a starting point for our thruster design. It takes approximately 1 ms for the gas to diffuse into the cone and reach a steady-state density, which gives a maximum repetition rate of 1 kHz to design the electronics around.

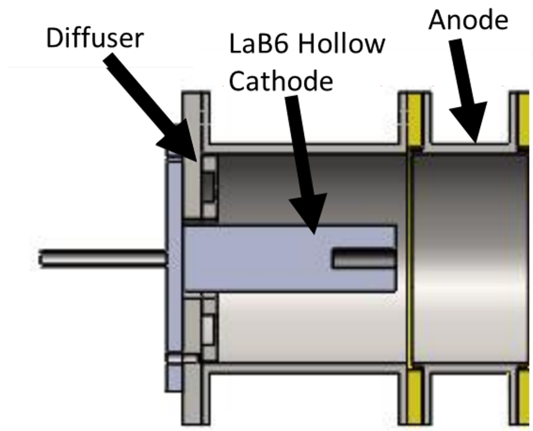

Fig. 4 A cutaway of the mechanical model of the plasma source

C. Bias Field System

We use 6 separate magnet windings to generate the steady bias field. The magnetic field was modelled in MAG-NET to determine the size and number of amp-turns for each coil. The magnitude of the bias field is approximately 400 G, and is angled at approximately 16 degrees relative to centerline. This size and magnitude was chosen based on heritage from past designs where there has been some experimental study of optimum cone angle[10].

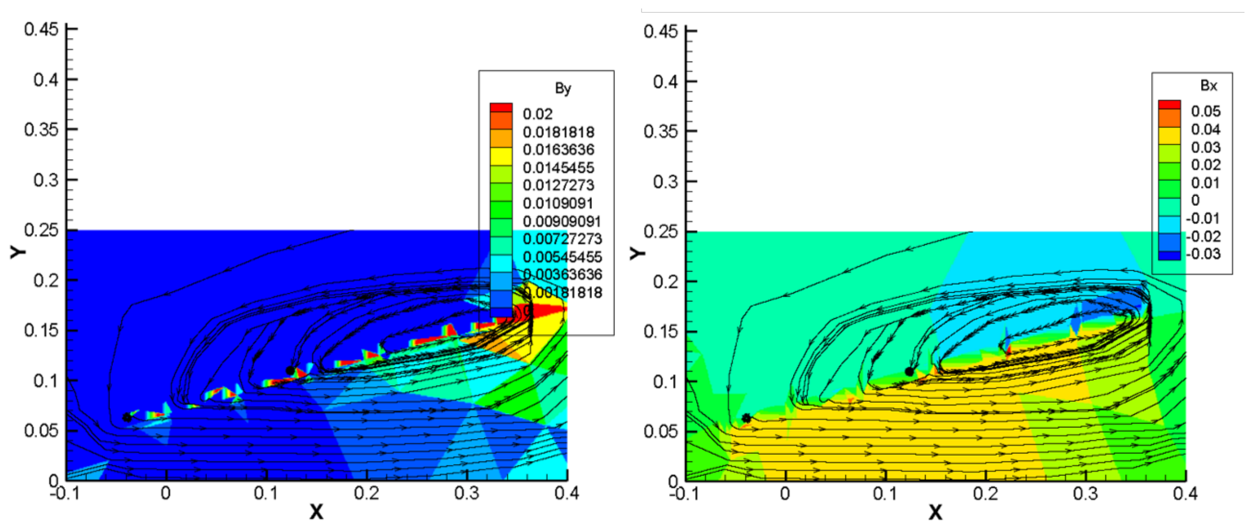

Fig. 5 MAG-NET simulations of the bias magnetic field. The radial component is shown on the left, and the axial component is on the right. Units are in Tesla

These bias coils are mounted on aluminum bobbins which form the body of the thruster. In addition to providing structure, the bobbins fill the role of axial magnetic flux conservers. As the FRC is formed and accelerated, it will seek to expand radially due to thermal pressure in the plasma, causing the magnetic field structure to expand outward as well. By having a conducting shell, any expansion of the magnetic field outside the cone will result in an eddy current in the shell, which will in turn induce a magnetic field to maintain a constant magnetic flux. This flux conservation is critical to FRC formation.

D. RMF Antennas

Each of the two antennas which nest inside the bobbin structure forms a Helmholtz pair with itself, producing a magnetic field in the radial direction when current is passed through. The antennas

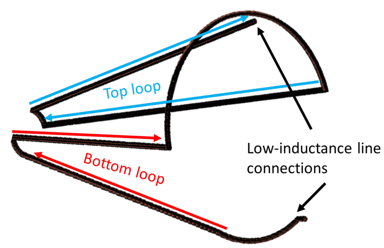

Fig. 6 One of the two RMF antennas which nest inside the cone of the thruster.

are clocked at 90 degrees relative to each other, which allows us to create a rotating radial magnetic field by pulsing them sinusoidally, 90 degrees out of phase with each other. This generates a rotating radial magnetic field given by Figure 4. The current which passes through the antennas is sized such that the centerline magnitude of the B-field is approximately 350 G. This is weak enough that the ion gyroradius is much larger than the scale length of the system thus allowing the electrons to rotate synchronously with the magnetic field lines.

The RMF antennas will be ringing at approximately 20 kHz to create the RMF frequency we desire, which corresponds to a skin depth of about .46 mm. Therefore, we use copper tubing as our conductor to take advantage of its two conducting faces. Additionally, water can be flowed through the copper tubing to prevent overheating in full rep-rated operation. To couple power into these antennas, we have designed and built custom low-inductance transmission lines. We require that the total inductance of the transmission line between the power processing unit and the antenna be less than 10% of the inductance of the antenna itself. This ensures that the pulsed power is stored in the antenna to be couple into the plasma, rather than along the line. Because each antenna has an inductance of approximately 2.5 μH, this limits the transmission line to 250 nH for its entire 22 ft length, or about 11 nH/ft. By holding pieces of copper sheet as close together as possible using heat shrink, we achieve 9 nH/ft using a broadside-coupled trace calculation. This puts the whole line at 130 nH for the entire length, or 5% of the antenna.

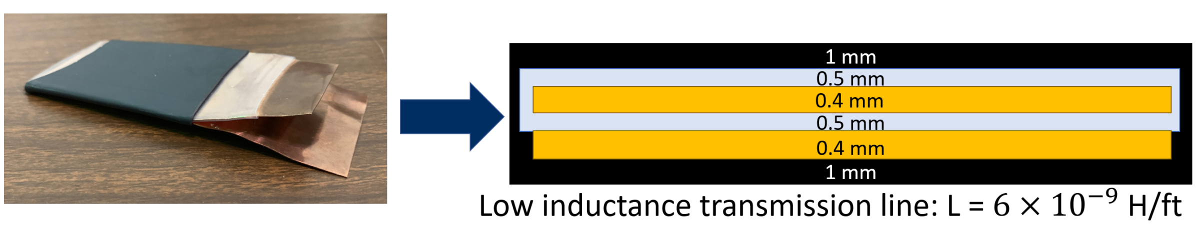

Fig. 7 Left: A photo of a section of low-inductance transmission line. Right: An illustration depicting of the cross section of the same.

E. Power-Processing Unit

To provide the 20 kHz power to the antennas at 1 kHz pulse rate, we have designed a custom power processing unit (PPU). The PPU consists of a 1 kHz low-pass filter to protect our 150 kW DC power supply from transients associated with the high frequency switching, and two boost circuits in parallel to power the antennas.

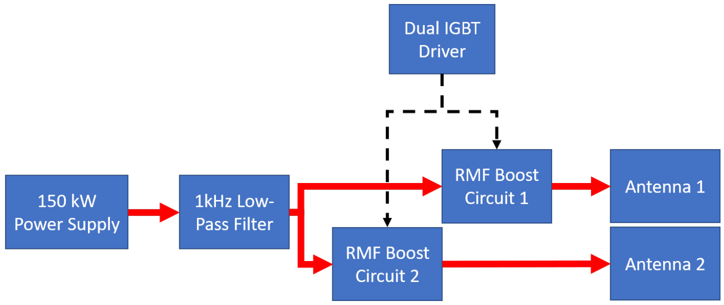

Fig. 8 A simplified block diagram of the PPU. Red solid lines indicate power transmission while dotted black indicates optical signal.

The boost circuit, in turn, consists of a high speed voltage doubler which uses a dual IGBT as a switch to deliver pulses at a specified repetition rate. A snubber protects the dual IGBT from switching transients which might cause damage. A safety switch allows us to safely discharge all power stored in the circuit after operation. The dual IGBTs and safety discharge switches are triggered optically by a separate custom driver circuit. This driver circuit takes desired repetition rate and phase delay between RMF antennas as inputs, and sends low-power signals to cause the IGBTs to open and close in appropriate sequence. All high-voltage components are optically isolated for safety. Water cooling is necessary for the PPU because of the high power levels involved. Inside the box, components are mounted on aluminum blocks which accept water flow. The charging inductors are large enough, however, that simply mounting them on a heat sink will not be sufficient. Instead, we have designed custom air-cored inductors which accept water cooling directly into the unit.

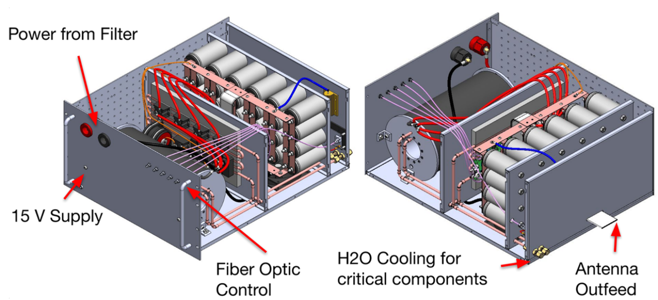

Fig. 9 A cutaway of the mechanical design of a single coil's PPU box. Two of these are stacked together along with a separate filter box.

VI. Conclusion

We presented an overview of RMF-FRC thrust mechanism theory and discussed our lumped circuit model in the context of thruster performance and design. We constructed a framework for validating our mutual inductance model and calibration for an emircal performance model that can be used to guide design and optimization studies. Using the goals set out for our test campaign, we detailed our design requirements and subsystems for our RMF-FRC test article. The thruster will be able to operate at various magnetic field strengths, pulse rates, and input power. The results of this test campaign will provide insight into the validity to our performance model and preliminary scaling laws that dictate thruster performance.

VII. Appendix

he full system of equations consists of Kirchoff's voltage law (KVL) for the RMF antennae, the azimuthal plasma current, and the flux conservers.

KVL for the RMF antennae is:

$$V_x(t) + R_e I_x(t) + (L_e + L_{RMF})\frac{dI_x(t)}{dt} = k\frac{d\Phi_x(t)}{dt} \tag{24}$$

$$V_y(t) + R_e I_y(t) + (L_e + L_{RMF})\frac{dI_y(t)}{dt} = k\frac{d\Phi_y(t)}{dt} \tag{25}$$

Here, terms denoted with x or y represent terms associated with the x- and y-direction RMF coils respectively. R_e and L_o are the parasitic resistance and inductance respectively. L_{RMF} is the RMF coils' inductance. $V_{x,y}$ is the voltage caused by the discharge of the capacitor banks and follows the relation:

$$\frac{dV_x(t)}{dt} = \frac{I_x(t)}{C} \tag{26}$$

$$\frac{dV_y(t)}{dt} = \frac{I_y(t)}{C} \tag{27}$$

$\phi_{x,y}$ is the flux coupled to the RMF antennae by the plasmoid. Per our previous study, the flux terms are calculated by solving for the magnetic fields produced by the axial plasmoid currents using Biot-Savart. We neglect the contribution of the plasmoid's own curents (i.e. self-inductance). The full expressions are:

$$\phi_x(t) = \frac{r_p(3{r_c}^2 + r_p)\gamma\mu_o(z_o - z(t))}{3\sqrt{2}\eta}\left[-\frac{dI_x(t)}{dt} + \frac{\Omega(t)^2}{2\big(1+\Omega(t)^2\big)}\omega_o I_y(t)\right] \tag{28}$$

$$\phi_y(t) = \frac{r_p(3{r_c}^2 + r_p)\gamma\mu_o(z_o - z(t))}{3\sqrt{2}\eta}\left[-\frac{dI_y(t)}{dt} + \frac{\Omega(t)^2}{2\big(1+\Omega(t)^2\big)}\omega_o I_x(t)\right] \tag{29}$$

Where, μ_o is the permittivity of free space, r_p is the radius of the plasmoid slug, r_c is the radius that the RMF antennae are set from centerline, z_o is the length of the acceleration region (thruster length), k is the coupling factor, and γ is defined as:

$$\gamma = \frac{B_{RMF,x}(t)}{I_x(t)} = \frac{B_{RMF,y}(t)}{I_y(t)} \tag{30}$$

Furthermore, Ω is the Hall parameter defined as:

$$\Omega^2 = \frac{1}{\eta^2 n^2 e^2}\left({B_{s,r}}^2 + \frac{1}{2}\gamma^2\Big(I_x(t)^2 + I_y(t)^2\Big)\right) \tag{31}$$

References

[1] Jahn, R. G., *Physics of Electric Propulsion*, McGraw-Hill Book Company, New York, 1968.

[2] Florenz, R. E., *The X3 100-KW Class Nested-Channel Hall Thruster: Motivation, Implementation, and Initial Performance*, Ph.D. thesis, University of Michigan, 2014.

[3] Hall, S., *Characterization of a 100-kW Class Nested-Channel Hall Thruster*, Ph.D. thesis, University of Michigan, 2017.

[4] Spence, B., White, S., Wilder, N., Gregory, T., Douglas, M., Takeda, R., Mardesich, N., Peterson, T., Hillard, B., Sharps, P., and Fatemi, N., "Next Generation UltraFlex Solar Array for NASAs New Millennium Program Space Technology 8," *2005 IEEE Aerospace Conference*, 2005, pp. 824–836.

[5] Mahoney, E., "In-Situ Resource Utilization," 2018.

[6] McKenna, K., "Equilibrium Constraints Applied to RMF-Driven Compact Toroid Devices," *Report No. LA-9024-MS, Los Alamos National Laboratory*, 1981.

[7] Blevin, H. A. and Thonemann, P. C., "Plasma confinement using an alternating magnetic field," *Nuclear Fusion Supplement, Part 1*, 1962, pp. 55.

[8] Weber, T., Slough, J., and Kirtley, D., "The Electrodeless Lorentz Force (ELF) Thruster Experimental Facility," *Review of Scientific Instruments*, 2012, pp. 83, 113509.

[9] Slough, J., "Pulsed Plasmoid Propulsion: The ELF Thruster," *31 International Electric Propulsion Conference*, 2009, pp. 1–24.

[10] Weber, T. E., *The Electrodeless Lorentz Force Thruster Experiment*, Ph.D. thesis, University of Washington, 2010.

[11] Jankovsky, R., Tverdokhlebov, S., and Manzella, D., "High Power Hall Thrusters," *35th Joint Propulsion Conference*, 1999, pp. AIAA–99–315745.

[12] Hill, C. S., "Preliminary Results on an Annular Field Reversed Configuration Translation Experiment," *IEPC-2011-281*, 2011.

[13] Eskridge, R. H., Fimognary, P. J., Martin, A. K., and Lee, M. H., "Design and Construction of the PT-1 Prototype Plasmoid Thruster," *AIP Conference Proceedings*, 2006, pp. 813, 474.

[14] Slough, J., Blair, A., Pihl, C., and Votroubek, G., "Magnetically Accelerated Plasmoid (MAP) Thruster - Initial Results and Future Plans," *IEPC-2007-16*, 2007.

[15] Woods, J. M., Jorns, B. A., , and Gallimore, A. D., "Circuit Modeling of Rotating Magnetic Field Field-reversed Configuration Thrusters," *AIAA-2018-4911*, 2018.

[16] Novac, B M, S. I. R. E. M. C. and P, S., "Studies of a Very High Efficiency Electromagnetic Launcher," *Journal of Physics D-Applied Physics*, , No. 35, 2002, pp. 1447–57.

[17] Bernardes, J. and Merrymann, S., "Parameter Analysis of a Single Stage Induction Mass Driver," *5th IEEE International Pulsed Power Conference*, Albuquerque, New Mexico, 1983.

[18] Martin, A. and Eskridge, R., "Electrical Coupling Efficiency of Inductive Plasma Accelerators," *Journal of Physics D-Applied Physics*, Vol. 38, No. 23, 2005, pp. 4168–4179.

[19] Hill, C., *Translation Studies on an Annular Field Reversed Configuration Device for Space Propulsion*, Michigan Technological University, PhD Dissertation, 2012.

[20] "Numerical Optimization of an Annular Field Reversed Configuration Translation Experiment," *31st International Electric Propulsion Conference*, Ann Arbor, Michigan, September 2009.

[21] Hugrass, W N, O. T. and Ohnishi, M., "Plasma-circuit Interactions in Rotating Magnetic Field Current Drive," *Plasma Physics and Controlled Fusion*, Vol. 50, February 2008, pp. 055008.

[22] "Scaling of FRC Thrusters with Neutral Entrainment," *8th JANNAF Spacecraft Propulsion Subcommittee Meeting*, Phoenix, Arizona, December 2016.

[23] Ji, H, Y. M. K. R. P. N. and Himura, H., "Studies of Global Stability of Field-Reversed Configuration Plasmas Using a Rigid Body Model," *Physics of Plasmas*, Vol. 5, No. 10, 1998, pp. 3685–3693.